Supporting information

Enhanced cathodic activity by tantalum inclusion at B-site of $La_{0.6}Sr_{0.4}Co_{0.4}Fe_{0.6}O_3$ based on structural property tailored *via* camphor-assisted solid-state reaction

Dingyu Xiong[a], Sefiu Abolaji Rasaki[a,c*], Yangpu Li[d], Liangdong Fan[d], Changyong Liu[a,b], and Zhangwei Chen[a,b,*]

[a]Additive Manufacturing Institute, Shenzhen University, Shenzhen, 518060, China.

[b]Guangdong Key Laboratory of Electromagnetic Control and Intelligent Robotics, Shenzhen University, Shenzhen, 518060, China.

[c]Department of Chemical and Petroleum Engineering, University of Calgary, 2500 University Drive NW, Calgary, Alberta, T2N1N4, Canada.

[d]College of Chemistry and Environmental Engineering, Shenzhen University, Shenzhen, 518060, China.

[*]Corresponding author email: chen@szu.edu.cn (Z. Chen)

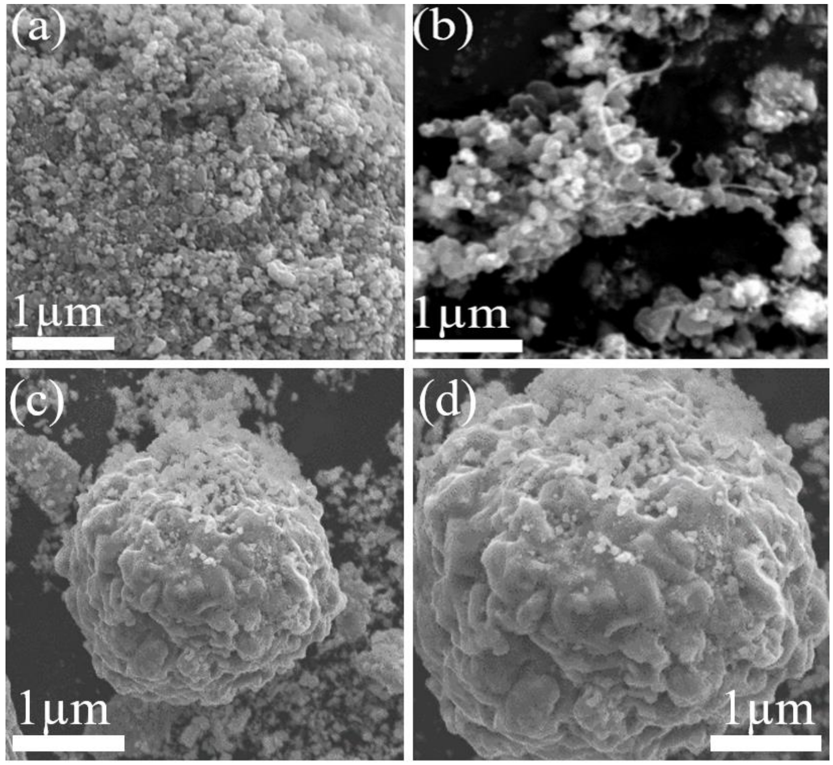

Fig. S1 SEM image (a) LSCF and (b) LSCFT before template removal from CSSR-derived materials. Each of the sample contains carbon which creates voids after removal via thermal treatment. SEM images of the samples prepared via traditional solid-state reaction (c) LSCF, and (d) LSCFT

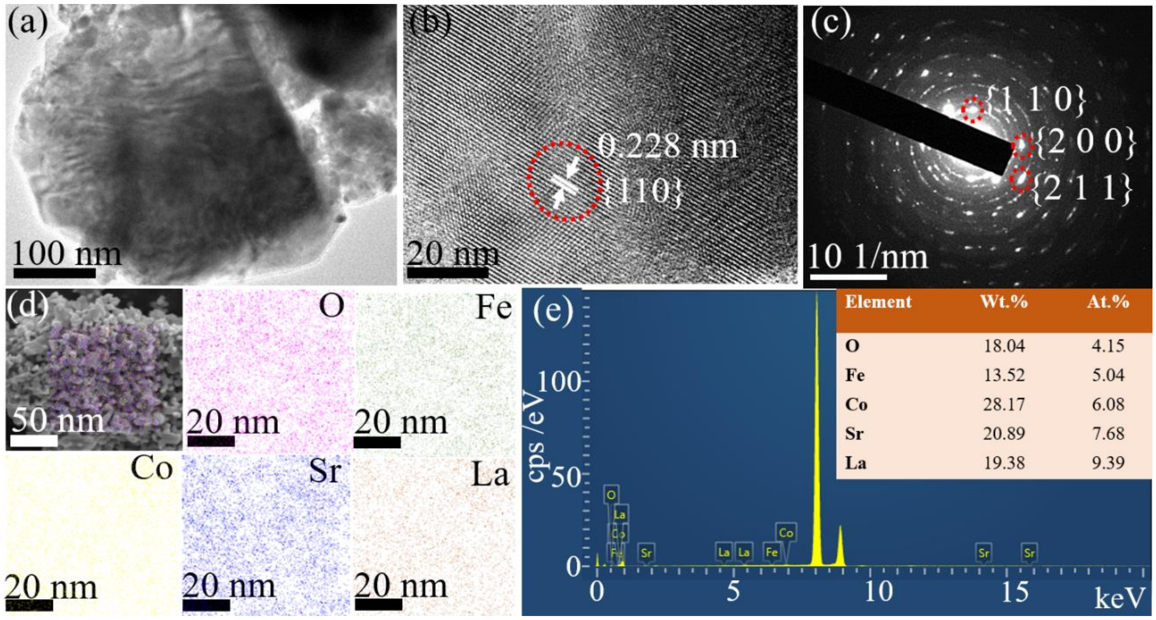

Fig. S2 (a) TEM images of the as-prepared LSCF, (b) High-resolution TEM of LSCF showing the lattice spacing of LSCF. (c) Selected area electron diffraction (SAED) indicating crystal planes of LSCF. (d) Energy dispersive X-ray spectroscopy (EDS) for element maps of LSCF, and (e) EDS graph of the LSCF showing the composition percentage of each element in the sample.

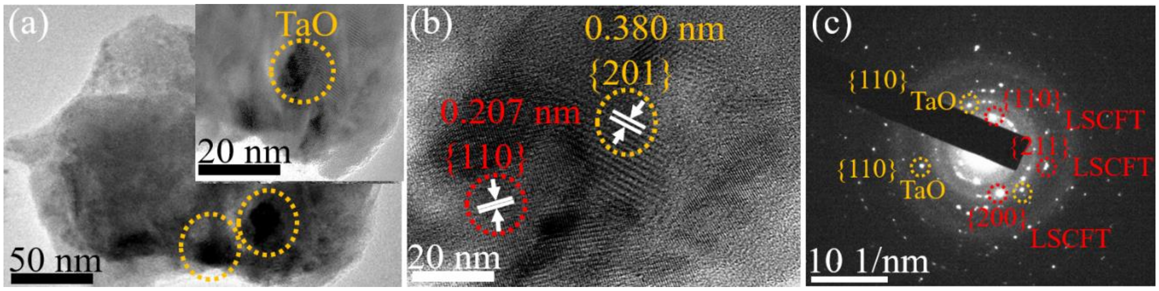

Fig. S3 (a) TEM images of LSCFT-1 showing the formation and distribution of excess tantalum oxide (TaO). (b) High resolution TEM of LSCFT-1 indicating the lattice spacing of the excessive TaO and single phase LSCFT. (c) Selected area electron diffraction (SAED) showing the crystal plane of TaO and LSCFT.

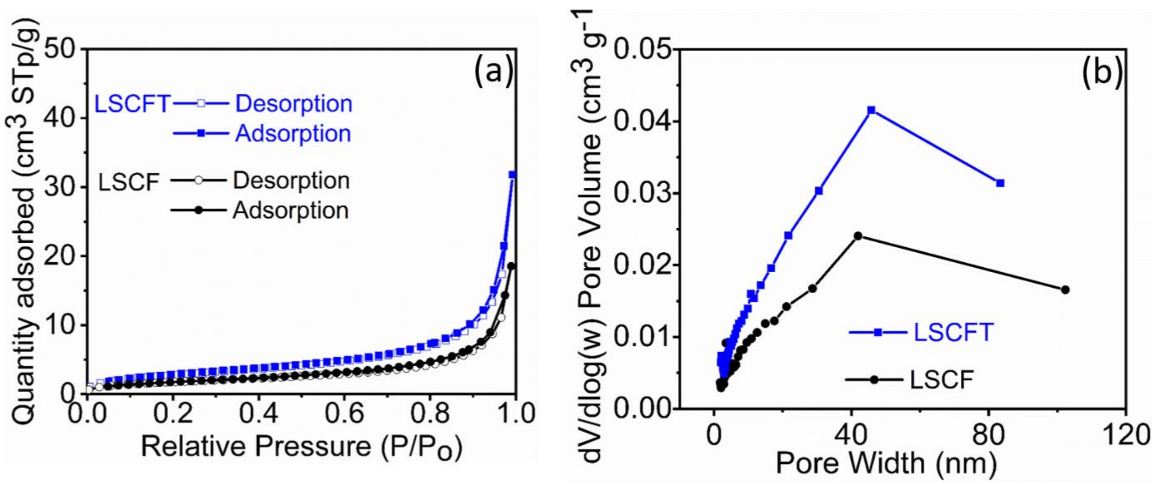

Fig. S4 Comparison of N_2 adsorption/desorption isotherm curves of the CSSR-derived LSCF and LSCFT (a) surface area, and (b) pore volume.

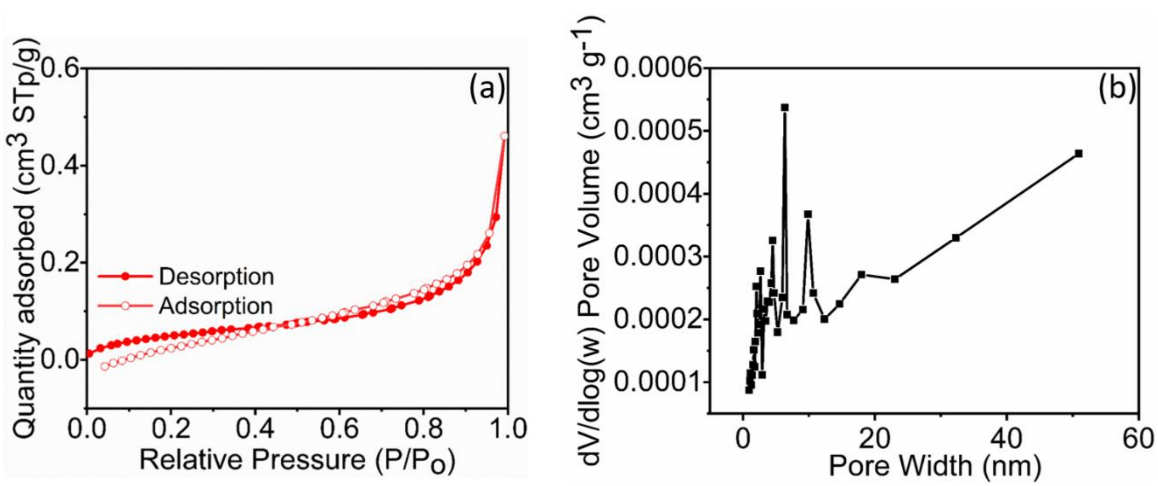

Fig. S5 N_2 adsorption/desorption isotherm curves of LSCF prepared via traditional solid-state reaction (a) surface area, and (b) pore volume**.**

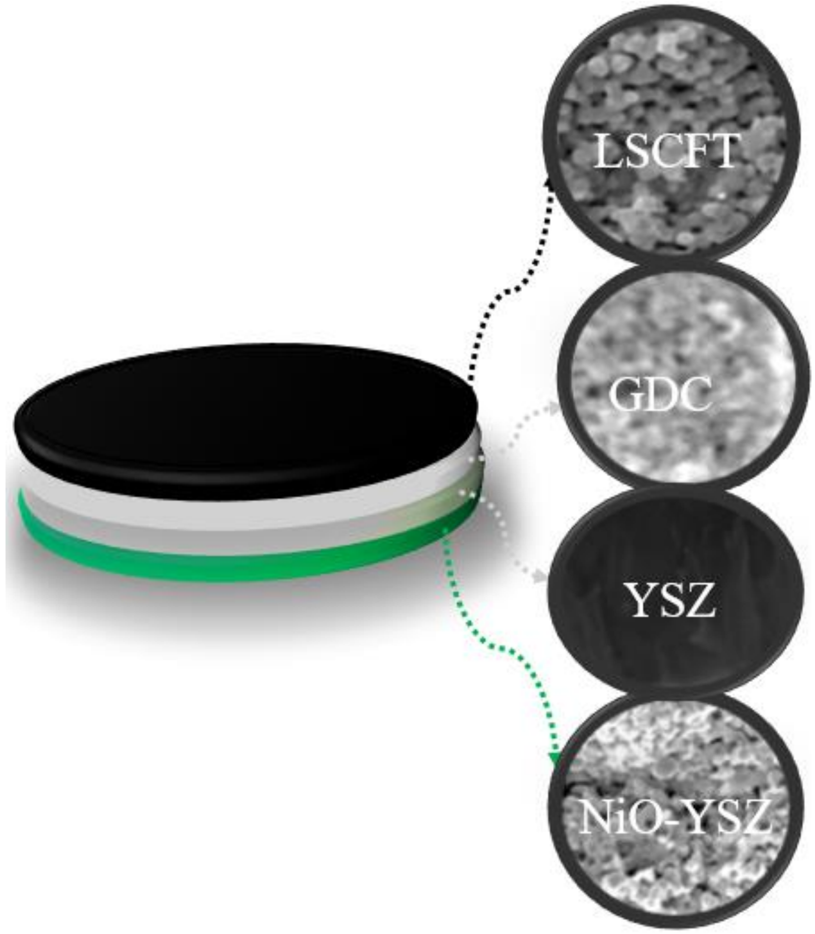

Fig. S6 Schematic illustration of the anode-supported single-cell with LSCFT cathode

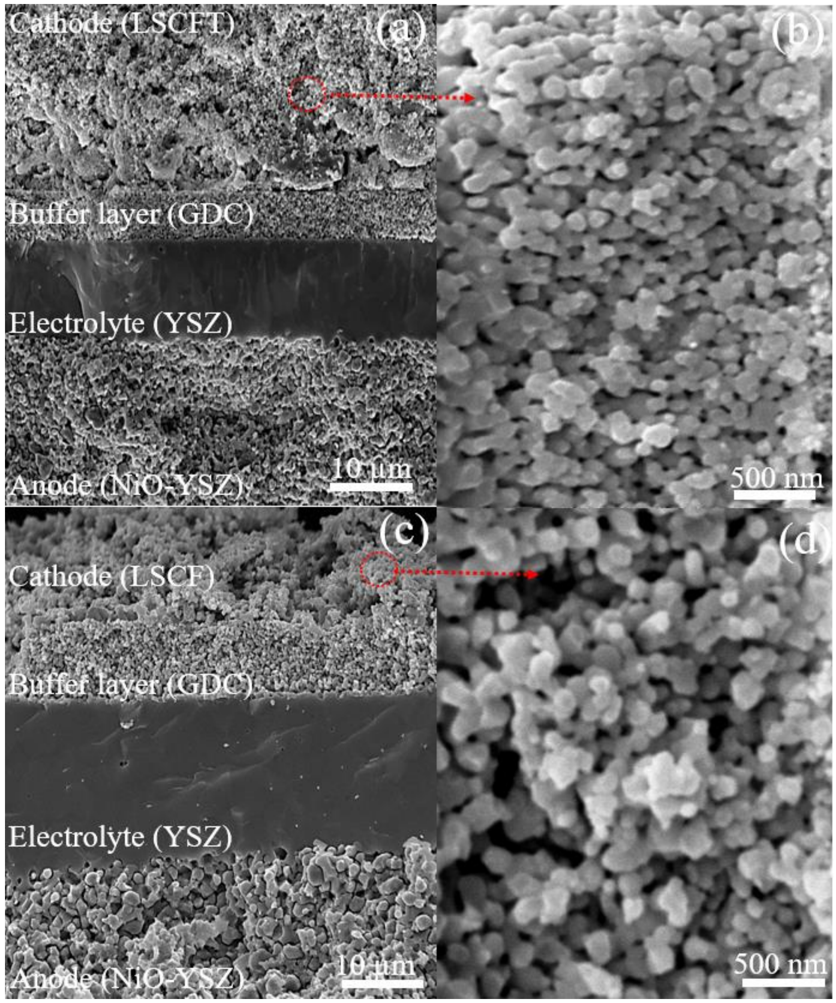

Fig. S7 SEM images of cross-sectional part of (a) single-cell with LSCFT cathode electrode, (b) LSCFT cathode, (c) single-cell with LSCF cathode electrode, and (d) LSCF cathode electrode. The images were taken after electrochemical performance test.

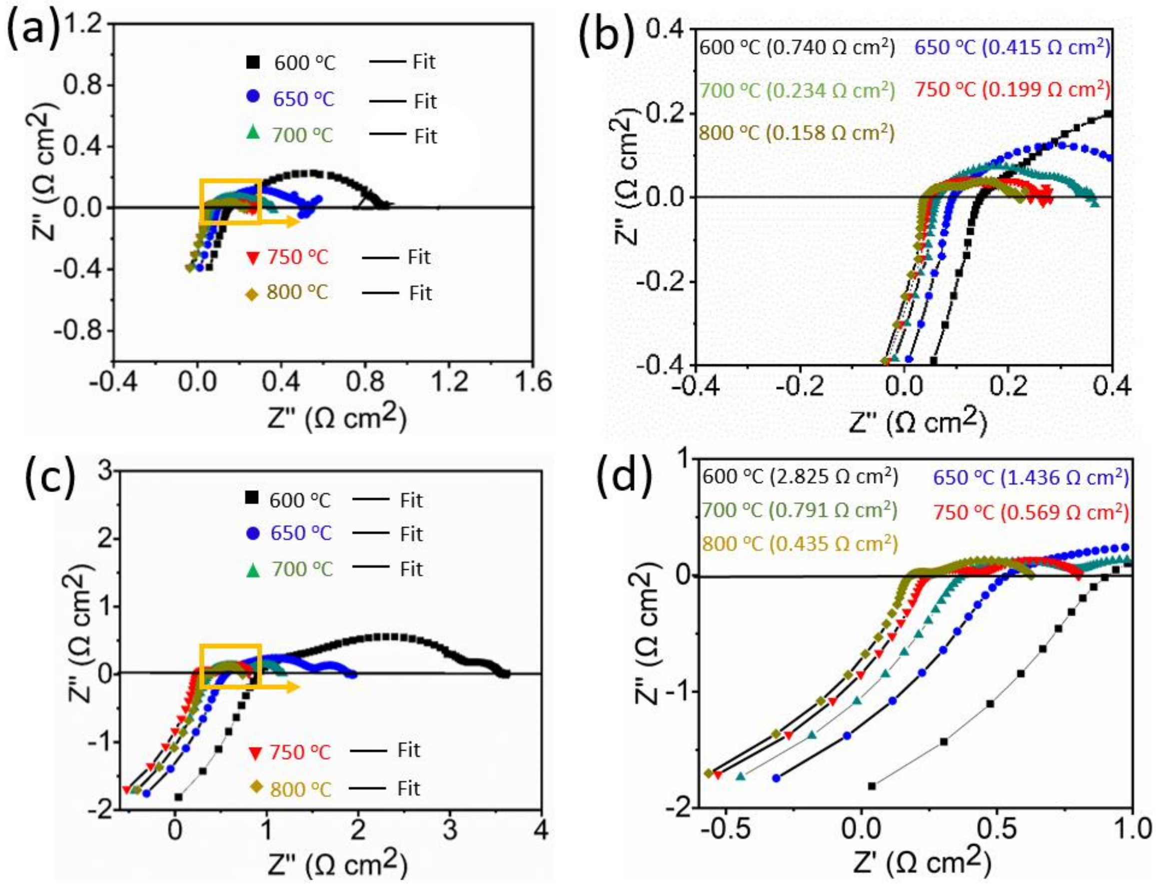

Fig. S8 EIS measurements in the air at 600-800 °C of (a-b) LSCFT and (c-d) LSCF in an anode-supported single-cell with the configuration of NiO-YSZ|YSZ|GDC|LSCFT and NiO-YSZ|YSZ|GDC|LSCF respectively

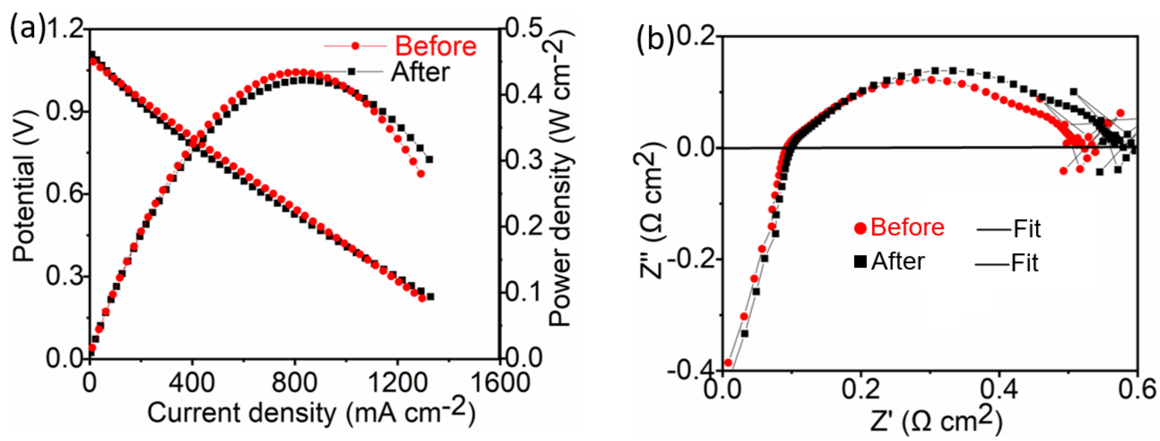

Fig. S9: (a) Current-voltage-power (I-V-P) curves after and before stability test for the anode-supported single-cell NiO-YSZ|YSZ|GDC with LSCFT cathode materials, and (b) EIS measurements in the air at 650 °C of the anode-supported single-cell NiO-YSZ|YSZ|GDC with LSCFT cathode materials before and after stability test.

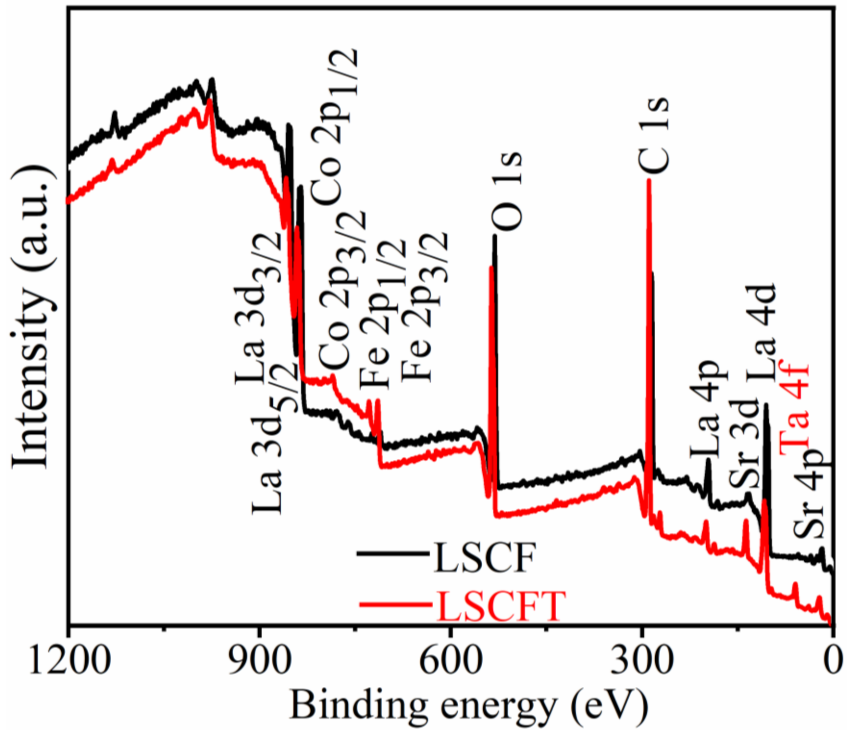

Fig. S10 Comparison of low-resolution XPS peaks of the LSCFT and LSCF.

Table. S1: Comparison of structural properties of LSCF and LSCFT.

Material	Cell parameter(Å)	Plane diameter (nm)
LSCFT-0	a = b = 5.445, c = 13.255	0.180
LSCFT-1	a=b=5.625 c=13.242	0.187
LSCFT-2	a=b=5.620 c=13.245	0.189
LSCF	a = b =5.456, c = 13.200	0.184

Table S2: Comparison of recent electrochemical performance of some of the doped LSCF or its composite as cathode material for SOFCs.

Cathode material	single cell composition	ASR@T_{min}	ASR@T_{max}	PPD@T_{min}	PPD@$T_{max.}$	Ref.
LSCF-CeO_2 composite	NiO-YSZ/YSZ/GDC/LSCF-CeO_2	0.154@600	0.031@700	685.1@600	1221.6@700	[1]
Cerium-doped LSCF ($La_{0.54}Ce_{0.06}Sr_{0.4}Co_{0.2}Fe_{0.8}O_3$)	$La_{0.54}Ce_{0.06}Sr_{0.4}Co_{0.2}Fe_{0.8}O_3$/GDC/$La_{0.54}Ce_{0.06}Sr_{0.4}Co_{0.2}Fe_{0.8}O_3$	0.820@650	0.037@800	-	-	[2]
Mo-doped LSCF ($La_{0.6}Sr_{0.4}Co_{0.2}Fe_{0.75}Mo_{0.05}O_{3-\delta}$)	$La_{0.6}Sr_{0.4}Co_{0.2}Fe_{0.75}Mo_{0.05}O_{3-\delta}$/GDC/$La_{0.6}Sr_{0.4}Co_{0.2}Fe_{0.75}Mo_{0.05}O_{3-\delta}$	-	0.149@700	-	-	[3]
Rh-doped LSCF	NiO-YSZ/YSZ/GDC/Rh-doped LSCF	0.468@650	0.169@800	600@650	1830@800	[4]
Pd-doped LSCF	NiO-YSZ/YSZ/GDC/Pd-doped LSCF	0.468@650	0.155@650	590@650	1990@800	[4]
LSCF-CGO composite	NiO-CGO/CGO/LSCF-CGO	-	-	121@500	240@600	[5]
GDC-LSCF composite	NiO-YSZ/YSZ/GDC/ GDC-LSCF	-	-	410@700	890@800	[6]
LSCF-GDC	NiO-YSZ/YSZ/LSCF-GDC	0.036@600	-	1500@650	3300@700	[7]
LSCF	NiO-YSZ/YSZ/GDC/LSCF	2.515@650	0.100@800	86@ 600	1270@800	This study
Ta-doped LSCF	NiO-YSZ/YSZ/GDC/Ta-doped LSCF	1.260@600	0.06@800	226@650	1374@800	This study

Note: ASR = area specific resistance ($\Omega\cdot cm^2$), PPD = peak power density ($mW\cdot cm^{-2}$), $T_{min.}$ = minimum temperature of electrochemical testing (°C), $T_{max.}$ = maximum temperature of electrochemical testing (°C), CGO = $Ce_{0.9}Gd_{0.1}O_{1.95}$.

Reference

[1] Zhang W, Wang H, Guan K, *et al.* $La_{0.6}Sr_{0.4}Co_{0.2}Fe_{0.8}O_{3-\delta}/CeO_2$ heterostructured composite nanofibers as a highly active and robust cathode catalyst for solid oxide fuel cells. *ACS Appl Mater Inter* 2019, **11**: 26830-26841.

[2] Zhou F, Liu Y, Zhao X, *et al.* Effects of cerium doping on the performance of LSCF cathodes for intermediate temperature solid oxide fuel cells. *Int J Hydrogen Energy* 2018, **43**: 18946-18954.

[3] Liu Y, Zhou F, Chen X, *et al.* Enhanced electrochemical activity and stability of LSCF cathodes by Mo doping for intermediate temperature solid oxide fuel cells. *J Appl Electrochem* 2021, **51**: 425-433.

[4] J.M. Serra, H.P. Buchkremer. On the nanostructuring and catalytic promotion of intermediate temperature solid oxide fuel cell (IT-SOFC) cathodes, *J Power Sources* 2007, **172**: 768-774.

[5] L.P. Sun, M. Rieu, J.P. Viricelle, *et al.* Fabrication and characterization of anode-supported single chamber solid oxide fuel cell based on $La_{0.6}Sr_{0.4}Co_{0.2}Fe_{0.8}O_{3}$- delta -$Ce_{0.9}Gd_{0.1}O_{1.95}$ composite cathode, *Int J Hydrogen Energy* 2014, **39**: 1014-1022.

[6] J.W. Yun, J. Han, S.P. Yoon, *et al.* $Ce_{0.8}Gd_{0.2}O_2$ modification on $La_{0.6}Sr_{0.4}Co_{0.2}Fe_{0.8}O_3$ cathode for improving a cell performance in intermediate temperature solid oxide fuel cells, *J Ind Eng Chem* 2011, **17**: 439-444.

[7] K. Develos-Bagarinao, T. Ishiyama, H. Kishimoto, *et al.* Nanoengineering of cathode layers for solid oxide fuel cells to achieve superior power densities, *Nat Commun* 2021, **12**: 1-12.